A Constitutive Description for Aluminum-0.1 Pct Magnesium Alloy under Hot Working Conditions

ELI S. PUCHI-CABRERA

The constitutive behavior of an aluminum 0.1 wt pct Mg alloy deformed in the temperature range of 573 to 823 K at strain rates between 0.001 and 100 s^{-1} is analyzed on the basis of the concept of the mechanical threshold stress (MTS), $\hat{\sigma}$, taking into consideration the contributions from the different strengthening mechanisms that could be present in this alloy, $\hat{\sigma}_i$, which include one component that arises from the interaction between dislocations and solute atoms, $\hat{\sigma}_s$, and another contribution from the interaction between mobile and forest dislocations, $\hat{\sigma}_D$. The evolution of $\hat{\sigma}_D$ is described in terms of a generalized form of an exponential-saturation equation, whereas the characterization of the ratio, $s_i(\dot{\varepsilon}, T)$, between the flow stress at any strain rate and temperature, and the two components $\hat{\sigma}_i$ is carried out by means of the phenomenological model advanced by Kocks and co-workers. It is shown that the experimental values of the flow stress as well as the work-hardening rate can be accurately described following this approach and that the maximum difference between the experimental and calculated values of such a parameter is less than ± 4 MPa. The analysis conducted from continuous stress-strain curves determined at constant temperature and strain rate indicates that the relaxation strain in the generalized form of the Sah *et al*. relationship displays a significant strain rate dependence. The inclusion of such a dependence into the analysis by means of a simple parametric relationship leads to an improvement in the accuracy of the prediction of the model.

I. INTRODUCTION

HOT working operations of metals and alloys are usually carried out as part of the entire deformation processing applied to such materials for the manufacture of either semifinished or finished products. During deformation at elevated temperatures and strain rates, as well as during the interpass times that characterize multiple pass deformation operations, extensive microstructural changes take place in the material, which, in turn, have a significant influence on its response during thermomechanical processing.

Under these deformation conditions, the mechanical behavior of the material becomes highly temperature and strain rate dependent and the change in flow stress with the strain applied could reflect either the occurrence of work hardening or softening. The characterization, as precisely as possible, of the flow stress behavior of the material is one of the essential aspects of microstructural control during hot working by means of the numerical modeling of the process involved. Such characterization requires the development of accurate constitutive equations capable of describing the change in flow stress during processing in terms of temperature, strain rate, and current microstructure.

As reported by Li *et al*.,[1] the resistance of the structure of a metal to deformation depends on a number of physical mechanisms, which include strain hardening, internal damage, texture, *etc*., that are present in the current state of the structure. Therefore, the use of internal state variable (ISV) constitutive models could be a plausible way of accomplishing the description of the flow stress of the material, by integrating the effect of the different mechanisms involved and representing them in terms of a small number of macroscopic internal state variables.

In this regard, Follansbee and Kocks[2] carried out an investigation on the axisymmetric deformation behavior of 99.99 pct pure Cu at strain rates in the range of 10^{-4} to 10^4 s^{-1}, employing the mechanical threshold stress (MTS) or flow stress at 0 K, $\hat{\sigma}$, as an internal state variable. In this study, the changes in $\hat{\sigma}$ with strain rate and strain were measured and the experimental results were analyzed on the basis of the model previously advanced by Mecking and Kocks,[3] that is to say, by describing the results at constant structure with thermal activation theory. The strain and strain rate evolution of $\hat{\sigma}$ were treated by means of the sum of dislocation generation and dynamic recovery process. A significant result of the investigation conducted by Follansbee and Kocks[2] was that the athermal dislocation accumulation rate, or stage II hardening rate, became a strong function of the strain rate at strain rates above 10^3 s^{-1}, which led to an apparent increased strain rate sensitivity, as observed from the change in the flow stress at a given strain, as a function of the logarithm of the strain rate.

In a subsequent study, Follansbee and Gray[4] investigated the deformation behavior of Ti-6Al-4V at temperatures between 76 and 495 K, strain rates between 0.001 and 3000 s^{-1}, and compressive strains up to 0.3. In this work, measurements of the yield stress as a function of test temperature, strain rate, and prestrain history were analyzed according to the model proposed by Mecking and Kocks.[3] Also, $\hat{\sigma}$ was used as an internal state variable and the contributions to it from the various strengthening mechanisms present in this material were analyzed. Follansbee and Gray[4] concluded that the constitutive equations based on the Kocks–Mecking model can predict both monotonic deformation behavior, as well as the response to path changes involving dramatic or gradual variations in

ELI S. PUCHI-CABRERA, Professor, is with the School of Metallurgical Engineering and Materials Science, Universidad Central de Venezuela, Caracas 1045, Venezuela, Contact e-mail: epuchi@reacciun.ve

Manuscript submitted July 12, 2002.

temperature and strain rate. It is important to mention that the approach followed in this work did not involve either the search of the values of the different parameters of the model, which yielded the closest agreement with the experimental results, or the determination of the strain dependence of these parameters.

Li *et al.*[1] also conducted an investigation in order to provide a critical comparison of different ISV models that had been previously proposed for describing the deformation of metals at elevated temperatures, over a wide range of strain rates. Such comparison led these authors to present a set of modified constitutive relations that were subsequently applied for the description of some experimental data obtained for aluminum 1100 and a fully dense high-purity aluminum. In this approach, the materials constants involved were determined by means of a nonlinear least-squares fitting procedure. It was reported that the occurrence of both work-hardening and softening behaviors in these materials, as a result of applying different strain rates at the same temperature, could be more effectively modeled by considering a nonlinear functional dependence of the effective stress, with respect to the internal state variables in the evolution relationship. The model advanced by these authors was also validated by means of studies conducted on the deformation of an aluminum gradient specimen.

More recently, Chen and Gray[5] conducted an investigation on the constitutive behavior of Ta and Ta-W alloys. The dependence of the yield stress of these materials on temperature and strain rate was found to decrease while the strain-hardening rate increased with the W alloying content. The MTS approach was adopted to model the stress-strain behavior, which was found to provide the best fitting results to the materials investigated.

Gray *et al.*[6] also carried out a study on the influence of grain size on the constitutive response of Monel 400 by means of the MTS model. According to the authors, this approach provided a robust constitutive description able to capture yielding, the large-strain work-hardening rate, and grain size effects simultaneously. In addition, this model satisfactorily addressed the experimentally observed transients due to strain rate or temperature-path dependency.

In a recent investigation, Puchi-Cabrera *et al.*[7] analyzed the mechanical behavior of aluminum with different alloying contents up to 1 wt pct, deformed under hot-working conditions. The exponential saturation equation earlier advanced by Voce[8,9] was employed for the description of the evolution of the MTS, whereas the model advanced by Kocks[10] was employed for the description of the ratio $s(\dot{\varepsilon}, T)$ of the flow stress at any temperature and strain rate, σ, and $\hat{\sigma}$. Puchi-Cabrera *et al.*[7] determined that the increase in the alloying content of aluminum gave rise to an increase in $\hat{\sigma}$ mainly due to the effect of the alloying elements on the saturation threshold stress, $\hat{\sigma}_s$, and less markedly through the athermal stress, σ_a. On the contrary, it was found that the increase in the alloying content gave rise to a decrease of the stage II or athermal work-hardening rate, θ_0. Thus, it was concluded that the dependence of the flow stress at any temperature and strain rate on the alloying content evolves from the dependence of both $s(\dot{\varepsilon}, T)$ and $\hat{\sigma}$ on such a content.

Thus, the present investigation has been conducted in order to analyze in more detail the constitutive response of an Al-0.1 pct Mg alloy in terms of the MTS as an ISV, taking into consideration the contribution from the different strengthening mechanisms that could take place in this alloy and to show the validity of the use of a generalized form of the exponential-saturation law proposed by Sah *et al.*[11] for the description of the evolution of the mechanical threshold.

II. DETAILS OF THE MODEL USED[2,4–6]

The model advanced by Mecking and Kocks[3] assumes that deformation takes place at temperatures below the diffusion-controlled regime and at strain rates below the dislocation drag or velocity-controlled regime. Also, it considers that deformation is controlled by the thermally activated interactions of dislocations with obstacles which as a first approximation can be represented by a linear expression of the form

$$\frac{\sigma}{\mu} = \frac{\sigma_a}{\mu} + \sum_{i=1}^{N_{obst}} \left[s_i\left(\dot{\varepsilon}, T\right) \left(\frac{\hat{\sigma}_i}{\mu_0} - \frac{\sigma_a}{\mu} \right) \right] \qquad [1]$$

In Eq. [1], σ represents the current flow stress; σ_a the athermal stress, which characterizes the rate-independent interactions of dislocations with long-range barriers (*e.g.*, grain boundaries); μ the temperature-dependent shear modulus at any finite temperature; N_{obst} the number of different obstacles that interact with dislocations; $\hat{\sigma}_i$ the different strengthening contributions to the mechanical threshold from such obstacles; μ_0 the shear modulus at 0 K; and $s_i(\dot{\varepsilon},T)$ the ratio of the current flow stress to the contribution $\hat{\sigma}_i$.

The ratio $s_i(\dot{\varepsilon},T)$ can be characterized from the phenomenological model advanced by Kocks *et al.*,[12] according to which

$$\dot{\varepsilon} = \dot{\varepsilon}_{Ki} \exp\left(\frac{\Delta G_i}{kT}\right) \qquad [2]$$

or

$$\dot{\varepsilon} = \dot{\varepsilon}_{Ki} \exp\left\{ \frac{-g_{0i}\mu \mathbf{b}^3}{kT} \left[1 - \left(\frac{\sigma_i/\mu}{\hat{\sigma}_i/\mu} \right)^{p_i} \right]^{q_i} \right\} \qquad [3]$$

from which it is readily shown that

$$s_i\left(\dot{\varepsilon}, T\right) = \frac{\sigma_i}{\hat{\sigma}_i} = \left\{ 1 - \left[\frac{kT \ln\left(\dot{\varepsilon}_{Ki}/\dot{\varepsilon}\right)}{g_{0i}\mu \mathbf{b}^3} \right]^{1/q_i} \right\}^{1/p_i} \qquad [4]$$

In the preceding equations, $\dot{\varepsilon}$ represents the effective strain rate; $\dot{\varepsilon}_{K_i}$ a constant; ΔG_i the activation free enthalpy or the Gibbs free energy of activation for the type of obstacle i; g_{0i} the normalized activation free enthalpy; k the Boltzmann constant; T the absolute temperature; **b** the Burgers vector; σ_i the applied stress, minus any athermal component; and p_i and q_i also constants that characterize the statistically averaged shape of the obstacle profile ($0 < p_i \leq 1$; $1 \leq q_i \leq 2$).

In the present case, the only obstacles that will be considered are solute atoms and forest dislocations, whose contributions to the mechanical threshold will be represented by $\hat{\sigma}_S$ and $\hat{\sigma}_D$, respectively. Therefore, Eq. [1] is reduced to the following expression:

$$\sigma = \sigma_a + \left(\hat{\sigma}_S \frac{\mu}{\mu_0} - \sigma_a\right) s_S\left(\dot{\varepsilon}, T\right) + \left(\hat{\sigma}_D \frac{\mu}{\mu_0} - \sigma_a\right) s_D\left(\dot{\varepsilon}, T\right) \quad [5]$$

That is to say

$$\sigma = \sigma_a + \left(\hat{\sigma}_S \frac{\mu}{\mu_0} - \sigma_a\right)\left\{1 - \left[\frac{kT \ln\left(\dot{\varepsilon}_{KS}/\dot{\varepsilon}\right)}{g_{0S}\mu \mathbf{b}^3}\right]^{1/q_S}\right\}^{1/p_S} + \left(\hat{\sigma}_D \frac{\mu}{\mu_0} - \sigma_a\right)\left\{1 - \left[\frac{kT \ln\left(\dot{\varepsilon}_{KD}/\dot{\varepsilon}\right)}{g_{0D}\mu \mathbf{b}^3}\right]^{1/q_D}\right\}^{1/p_D} \quad [6]$$

In the current investigation, following the work of Follansbee and Gray,[4] it has been assumed that $p_S = 1$, $q_S = 2$, $p_D = 2/3$, and $q_D = 1$.

The Follansbee and Kocks model[2] assumes that the structure evolution can be described by an expression such as

$$\theta = \theta_0\left[1 - F\left(\frac{\hat{\sigma}_D - \sigma_a}{\hat{\sigma}_{Ds} - \sigma_a}\right)\right] \quad [7]$$

where θ represents the strain-hardening rate, $d\hat{\sigma}_D/d\varepsilon$; θ_0 the stage II or athermal work-hardening rate, that is to say, the hardening due to dislocation accumulation; $\hat{\sigma}_{Ds}$ the mechanical threshold stress at zero strain-hardening rate or saturation threshold stress; and F a function chosen to fit the particular data measured experimentally.

In the present case, it is considered that during deformation, microstructural evolution occurs only by the accumulation of dislocations during strain hardening and that the hardening rate can be modeled by the evolution of the MTS for dislocation/dislocation interactions by means of a generalized form of the exponential-saturation law advanced by Sah *et al.*,[11] which in differential form is given by

$$\theta = \theta_0\left(\frac{\hat{\sigma}_{Ds} - \sigma_a}{\hat{\sigma}_D - \sigma_a}\right)^{1/n-1}\left[1 - \left(\frac{\hat{\sigma}_D - \sigma_a}{\hat{\sigma}_{Ds} - \sigma_a}\right)\right]^{1/n} \text{ and } \theta_0 = \frac{n(\hat{\sigma}_{Ds} - \sigma_a)}{\varepsilon_r} \quad [8]$$

which after integration, is simply expressed as

$$\hat{\sigma}_D = \sigma_a + (\hat{\sigma}_{Ds} - \sigma_a)\left[1 - \exp\left(-\frac{\varepsilon}{\varepsilon_r}\right)\right]^n \quad [9]$$

where ε_r represents the relaxation strain, that is to say, the strain required to achieve a certain fraction of the maximum hardening attainable, represented by the difference $(\hat{\sigma}_{Ds} - \sigma_a)$ and n a constant in the range of approximately 0.1 to 0.5. However, in general, the differential form of the preceding equation is more convenient since it implies that strain is not assumed to be a state variable. In Eq. [9], ε represents the strain applied to the material.

It is important to point out that the model advanced by Mecking and Kocks[3] considers, as a fundamental basis, that the athermal dislocation accumulation rate is the variable that exerts the major effect on the initial part of the stress-strain curve. On the contrary, saturation behavior of the flow stress at elevated strains is expected to be affected mainly by dislocation rearrangements, features that are fulfilled by the hardening law employed in the present constitutive description.

Also, the model used in the current investigation considers that the contribution to the MTS from dislocation/dislocation interactions, $\hat{\sigma}_D$, is a function of temperature and strain rate and that it can be described in terms of these two variables by means of the model earlier advanced by Kocks:[10]

$$\ln\left(\frac{\dot{\varepsilon}}{\dot{\varepsilon}_{KDs}}\right) = \frac{\mu \mathbf{b}^3 g_{0Ds}}{kT} \ln\left(\frac{\hat{\sigma}_{Ds}}{\hat{\sigma}_{KDs}}\right) \quad [10]$$

where $\dot{\varepsilon}_{KDs}$ represents a material constant and g_{0Ds} another normalized activation-free enthalpy related to the extrapolation of $\hat{\sigma}_{Ds}$.

III. ANALYSIS AND DISCUSSION

The present investigation has been carried out employing the data previously reported by Prasad and Sasidhara[13] for Al-0.1 pct Mg. The flow stress, strain, strain rate, and temperature data for this material, provided by these authors, are presented in tables in which the flow stress, determined under axisymmetric compression conditions, is given at strain intervals of 0.1 in the temperature range 573 to 823 K and strain rates between 0.001 and 100 s^{-1}.

According to the authors, all the flow stress data have already been corrected for the adiabatic temperature rise during deformation, by applying a linear interpolation between log (σ) and $1/T$ values. The temperature was measured by inserting a fine thermocouple in a 0.8-mm-diameter hole reaching the center of the compressive specimens, which allowed the measurement of the actual temperature of the specimens.

The first step in the analysis of the experimental data consisted in the fit of the generalized expression of the Sah *et al.* law,[11] in differential form, to the current work-hardening rate obtained from the current stress-strain data, determined at different temperatures and strain rates. The term θ was represented as a function of the current flow stress and both parameters were normalized by $\mu(T)$. As is shown in Figures 1 through 4, only for the data at 573, 673, 723, and 823 K, and all the strain rates, the relationship between these parameters is highly nonlinear and can be described satisfactorily by means of Eq. [8] applied to the current flow stress values:

$$\theta = \theta_0\left(\frac{\sigma_s - \sigma_a}{\sigma - \sigma_a}\right)^{1/n-1}\left[1 - \left(\frac{\sigma - \sigma_a}{\sigma_s - \sigma_a}\right)\right]^{1/n} \quad [11]$$

$$\theta_0 = \frac{n(\sigma_s - \sigma_a)}{\varepsilon_r} \quad [12]$$

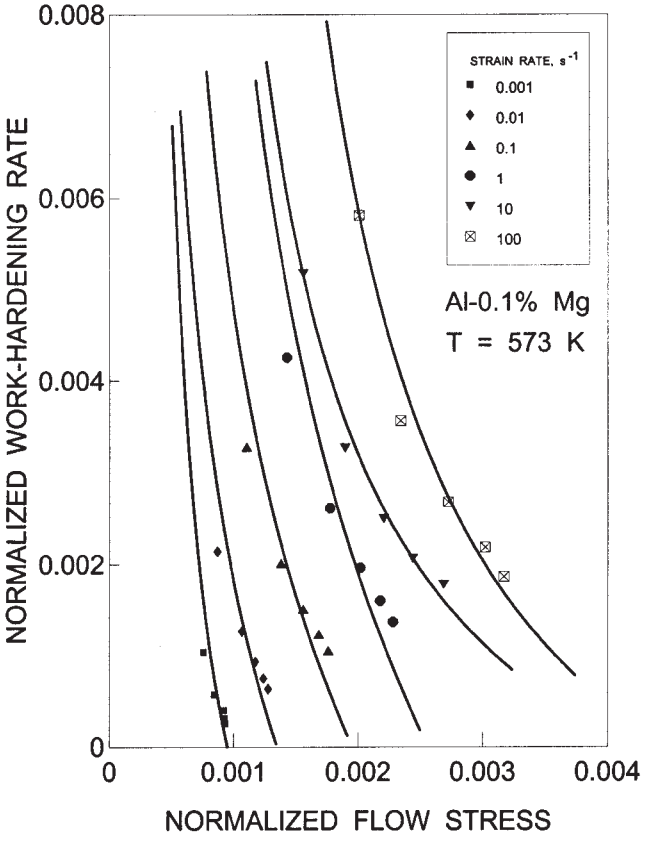

Fig. 1—Change in the normalized values of the current work-hardening rate as a function of the normalized values of the current stress, at 573 K and different strain rates. The solid line shows the fit of Eq. [13] in differential form to the experimental data points.

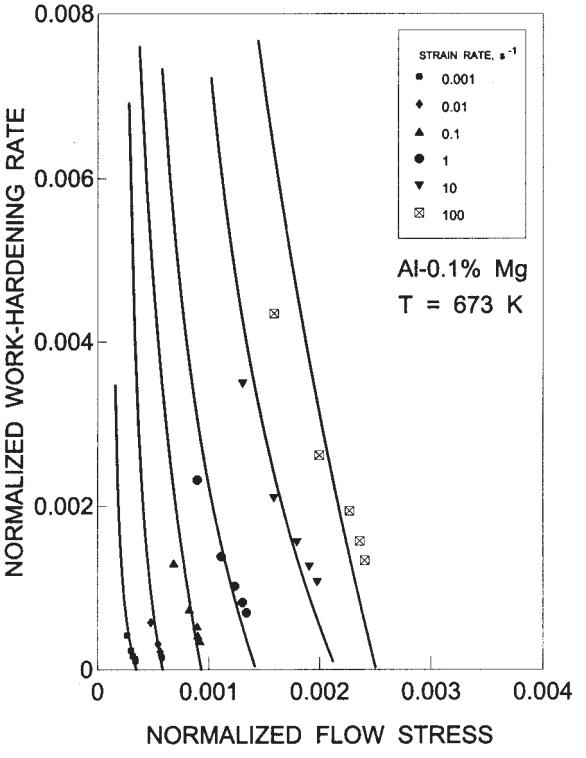

Fig. 2—Change in the normalized values of the current work-hardening rate as a function of the normalized values of the current stress, at 673 K and different strain rates. The solid line shows the fit of Eq. [13] in differential form to the experimental data points.

In the preceding equations, σ represents the current flow stress and σ_s the current saturation stress. The integrated form of the generalized law employed for this purpose is simply expressed as

$$\sigma = \sigma_a + (\sigma_s - \sigma_a)\left[1 - \exp\left(-\frac{\varepsilon}{\varepsilon_r}\right)\right]^n \qquad [13]$$

At this point, it is important to point out that while Eqs. [8] and [9] refer to the evolution of the MTS, Eqs. [11] through [13] refer to the evolution of the current flow stress. All the parameters involved in Eq. [13] can be readily determined by means of a least-squares method, that is to say, by minimizing the quadratic difference between the flow stress values given by Eq. [13] and the experimental ones. Therefore, the second step in the analysis of the present data consisted in the determination of all these parameters, and for this purpose, the objective function can be simply defined as

$$\Phi_1 = \sum_{i=1}^{N}\left\{\sigma_i - \sigma_a - \left(\sigma_s - \sigma_a\right)\left[1 - \exp\left(\frac{\varepsilon_i}{\varepsilon_r}\right)\right]^n\right\}^2 \qquad [14]$$

where N represents the number of experimental points for each stress-strain curve at every condition of temperature and strain rate. The value of the parameters σ_a, σ_s, ε_r, and n can be readily determined by solving the system of equations that result from the condition of minimization of the preceding equation, that is to say.

$$\frac{\partial \Phi_1}{\partial \sigma_a} = 0;\ \frac{\partial \Phi_1}{\partial \sigma_s} = 0;\ \frac{\partial \Phi_1}{\partial \varepsilon_r} = 0;\ \frac{\partial \Phi_1}{\partial n} = 0 \qquad [15]$$

Due to the lack of data below effective strains of 0.1 and according to the flow stress values reported at 823 K and low strain rates, the search interval for the parameter σ_a was restricted to the span 1 to 3 MPa. Table I summarizes the results of the fit of Eq. [13] to the experimental flow stress data, which allowed the computation of the parameters σ_a, σ_s, ε_r, and n for every condition of temperature and strain rate, whereas Figures [5] through [8] illustrate, as solid lines, the description provided by this hardening law to the experimental data.

In general, it can be seen that most of the curves present a typical work-hardening behavior in the strain interval of interest, as well as a marked trend to attain a saturation condition as the strain applied to the material increases. As expected, the rate at which saturation is achieved is a strong function of temperature and strain rate. As the deformation temperature increases and the strain rate decreases, saturation is attained after a shorter strain transient, which is clearly reflected in the stress-strain curves shown in Figures 5 through 8. It can be observed that Eq. [13] describes quite satisfactorily the experimental data under any condition of temperature and strain rate, which justifies

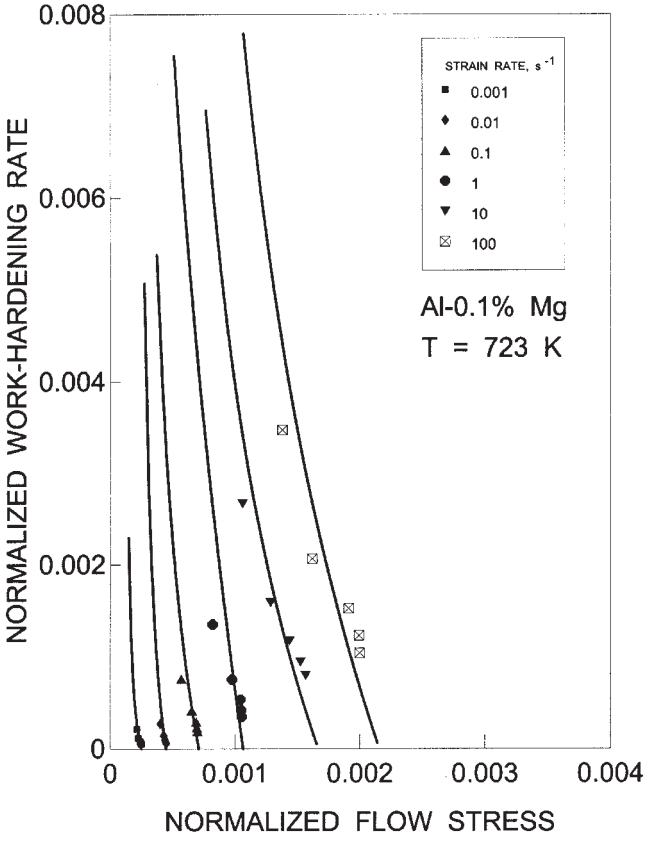

Fig. 3—Change in the normalized values of the current work-hardening rate as a function of the normalized values of the current stress, at 723 K and different strain rates. The solid line shows the fit of Eq. [13] in differential form to the experimental data points.

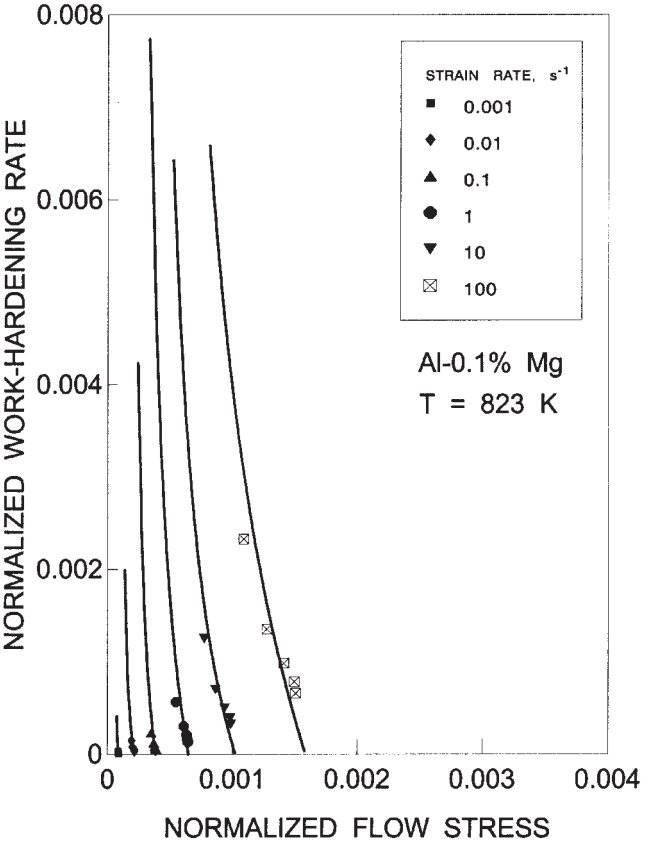

Fig. 4—Change in the normalized values of the current work-hardening rate as a function of the normalized values of the current stress, at 823 K and different strain rates. The solid line shows the fit of Eq. [13] in differential form to the experimental data points.

its use for the description of the evolution of the mechanical threshold.

The third step in the present analysis consisted in the actual application of the MTS model already described in Section II. Thus, in order to determine the different parameters involved in the constitutive description of this material, from Eqs. [6], [9], and [10], it is necessary to define a second objective function Φ_2 of the form

$$\Phi_2 = \sum_{i=1}^{Nr} \left\{ \sigma_i - \sigma_i^{comp} \right\}^2 \qquad [16]$$

with

$$\sigma_i^{comp} = \sigma_a + \left(\hat{\sigma}_S \frac{\mu_i}{\mu_0} - \sigma_a \right) \left\{ 1 - \left[\frac{kT_i \ln\left(\dot{\varepsilon}_{KS}/\dot{\varepsilon}_i \right)}{g_{0S}\mu_i \mathbf{b}^3} \right]^{1/q_S} \right\}^{1/p_S} + \left(\hat{\sigma}_{Di} \frac{\mu_i}{\mu_0} - \sigma_a \right) \left\{ 1 - \left[\frac{kT_i \ln\left(\dot{\varepsilon}_{KD}/\dot{\varepsilon}_i \right)}{g_{0D}\mu_i \mathbf{b}^3} \right]^{1/q_D} \right\}^{1/p_D} \qquad [17a]$$

$$\mu_i = 29{,}573.3 - 14.4T_i, \text{ MPa} \qquad [17b]$$

and

$$\hat{\sigma}_{Di} = \sigma_a + (\hat{\sigma}_{Dsi} - \sigma_a) \left[1 - \exp\left(-\frac{\varepsilon_i}{\varepsilon_{ri}} \right) \right]^n$$

$$\varepsilon_{ri} = \varepsilon_{r0} + \varepsilon_{r1} (\dot{\varepsilon}_l)^{m_r}$$

$$\ln\left(\frac{\dot{\varepsilon}_l}{\dot{\varepsilon}_{KDs}} \right) = \frac{\mu_i \mathbf{b}^3 g_{0Ds}}{kT_i} \ln\left(\frac{\hat{\sigma}_{Dsi}}{\hat{\sigma}_{KDs}} \right) \qquad [18]$$

and to solve simultaneously the system of nonlinear equations that renders the minimization of such a function:

$$\frac{\partial \phi_2}{\partial \sigma_a} = 0;\ \frac{\partial \phi_2}{\partial \hat{\sigma}_S} = 0;\ \frac{\partial \phi_2}{\partial \dot{\varepsilon}_{KS}} = 0;\ \frac{\partial \phi_2}{\partial g_{0S}} = 0;\ \frac{\partial \phi_2}{\partial \dot{\varepsilon}_{KD}} = 0;$$
$$\frac{\partial \phi_2}{\partial g_{0D}} = 0;\ \frac{\partial \phi_2}{\partial \varepsilon_{r0}} = 0;\ \frac{\partial \phi_2}{\partial \varepsilon_{r1}} = 0;\ \frac{\partial \phi_2}{\partial m_r} = 0; \qquad [19]$$
$$\frac{\partial \phi_2}{\partial n} = 0;\ \frac{\partial \phi_2}{\partial \varepsilon_{KDs}} = 0;\ \frac{\partial \phi_2}{\partial g_{0Ds}} = 0;\ \frac{\partial \phi_2}{\partial \hat{\sigma}_{KDs}} = 0$$

The expression for the temperature dependence of the shear modulus in Eq. [17] was derived from the data published by Sutton[14] and quoted by Kocks,[10] for aluminum.

It is important to point out that the present analysis differs from previous studies,[2,4–6] also conducted on the basis of the use of the MTS model, in several ways, which include the following: (1) the use of the generalized form of the

Table I. Material Parameters Involved in the Generalized Form of the Exponential-Saturation Law Proposed Sah *et al.*

σ_a, MPa	σ_s, MPa	ε_r	n	T, K	$\dot{\varepsilon}$, s^{-1}
1.0	20.2	0.16	0.32	573	0.001
1.0	28.8	0.24	0.43	573	0.01
2.3	41.7	0.33	0.47	573	0.1
3.0	54.6	0.35	0.46	573	1
3.0	88.2	1.30	0.41	573	10
3.0	94.8	1.07	0.36	573	100
1.0	10.7	0.14	0.31	623	0.001
1.0	18.8	0.20	0.34	623	0.01
1.0	29.9	0.24	0.44	623	0.1
3.0	41.8	0.52	0.38	623	1
3.0	60.5	0.52	0.42	623	10
3.0	63.9	0.31	0.48	623	100
1.0	6.9	0.21	0.34	673	0.001
1.0	11.6	0.15	0.31	673	0.01
1.0	18.6	0.14	0.51	673	0.1
1.0	28.3	0.24	0.44	673	1
2.5	42.7	0.30	0.44	673	10
1.0	49.8	0.18	0.56	673	100
1.0	4.8	0.18	0.26	723	0.001
1.0	8.5	0.11	0.24	723	0.01
1.0	13.6	0.14	0.36	723	0.1
1.0	20.4	0.10	0.57	723	1
1.1	32.0	0.26	0.43	723	10
1.5	41.3	0.25	0.44	723	100
1.0	4.9	3.01	0.35	773	0.001
1.0	6.0	0.14	0.23	773	0.01
1.0	9.7	0.15	0.29	773	0.1
1.0	14.7	0.17	0.33	773	1
2.0	24.2	0.31	0.38	773	10
1.0	31.0	0.19	0.40	773	100
1.0	1.6	0.13	0.23	823	0.001
1.0	3.8	0.14	0.25	823	0.01
1.0	6.8	0.11	0.24	823	0.1
1.0	11.5	0.13	0.29	823	1
1.5	18.1	0.23	0.31	823	10
1.1	28.1	0.23	0.38	823	100

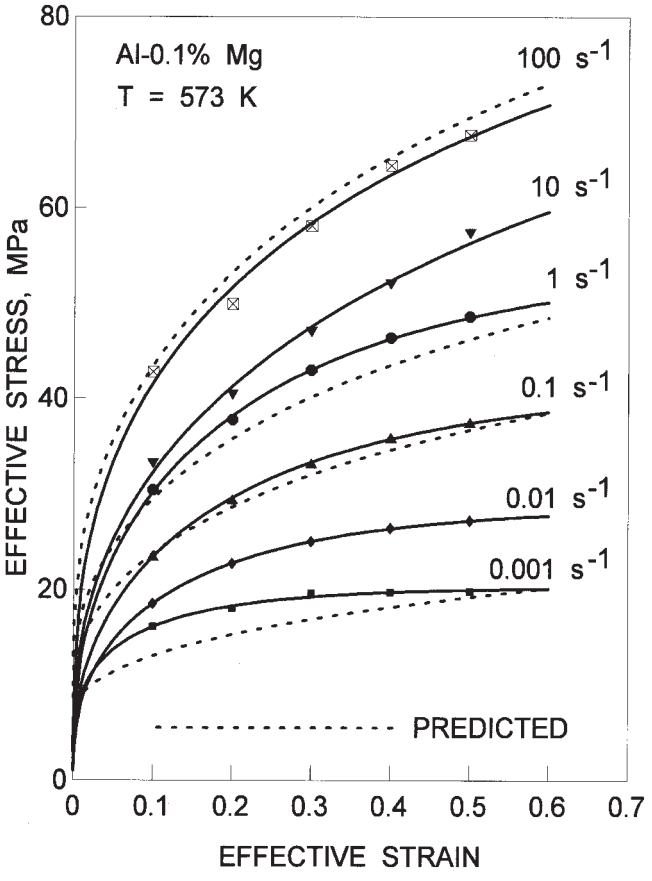

Fig. 5—Change in the current flow stress with strain at 573 K and different strain rates. The solid lines represent the optimization of the experimental data and the dotted lines the predictions of the constitutive equation proposed.

exponential-saturation law earlier advanced by Sah *et al*. for the description of the evolution of the mechanical threshold; (2) the inclusion in this description of a strain rate dependence of the relaxation strain; and (3) the use of stress, strain, strain rate, and temperature values obtained from continuous stress-strain curves determined under hot-working conditions, rather than curves obtained at low temperatures as in the previous analysis. The reasons that led to the inclusion of a strain rate dependence of the relaxation strain will be discussed later in the present section. Table II summarizes the results of this calculation and Figures [5] through [8] also illustrate as dotted lines the computed curves for some deformation conditions. In general, it can be observed that the description of the experimental data is quite satisfactory, since most of the optimized curves (solid lines fitted to Eq. [13]) are closely followed.

Therefore, the current flow stress of the material is described as a function of the deformation temperature, strain rate, and microstructure, the latter represented by the MTS, an internal state variable that in the present case is assumed to have two different components: one from the interaction of dislocations and solute atoms and another from the interaction between mobile and forest dislocations. The evolution of the microstructure at 0 K is described by means of a work-hardening law that also provides a very good description of the change in the current work-hardening rate with current stress. However, as was pointed out previously, a further assumption made in the present investigation is that at 0 K the component of the mechanical threshold that arises from the interaction between dislocations can also be affected by the strain rate through the relaxation strain, which has been expressed by means of a simple parametric relationship as a function of $\dot{\varepsilon}$ in Eq. [18].

The previous work conducted by Follansbee and Kocks[2] in copper also reported that in the strain rate range of approximately 10^{-4} to 10^{2} s^{-1}, the athermal work-hardening rate varied linearly with the logarithm of the strain rate, whereas at higher strain rates, a marked nonlinear increase took place. This phenomenon was explained on the basis of the limiting dislocation velocity and the average distance between obstacles, which would be inversely proportional to the strain rate applied to the material. Thus, given the relationship between the athermal work-hardening rate and the relaxation strain presented in Eq. [8], it also seems plausible to propose the existence of a similar dependence of ε_r on $\dot{\varepsilon}$, which has been confirmed in this work. This approach was found to be more satisfactory in terms of the computed value of the objective function Φ_2 with and without taking into consideration the strain rate dependence of the relaxation strain. If ε_r is considered to be

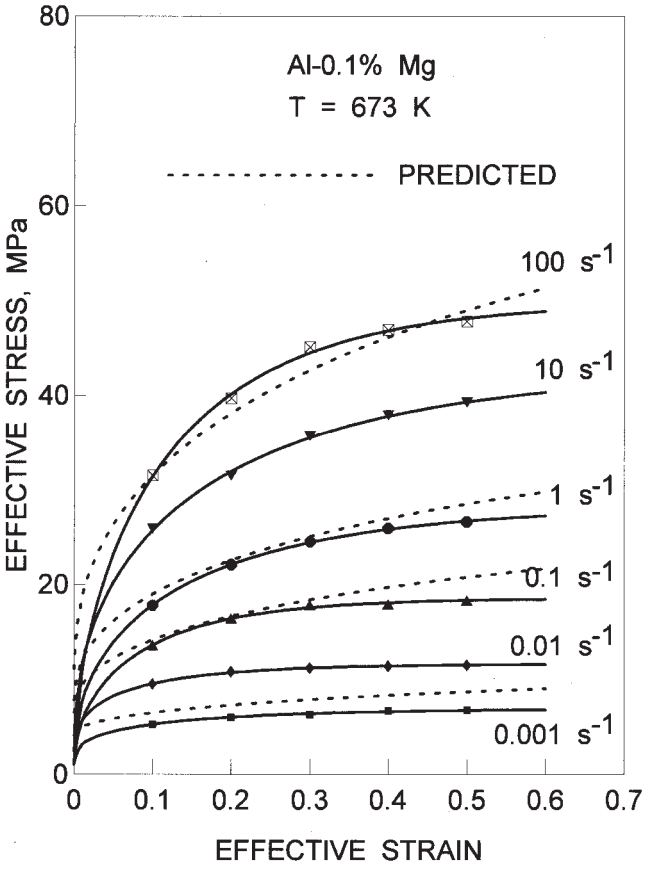

Fig. 6—Change in the current flow stress with strain at 673 K and different strain rates. The solid lines represent the optimization of the experimental data and the dotted lines the predictions of the constitutive equation proposed.

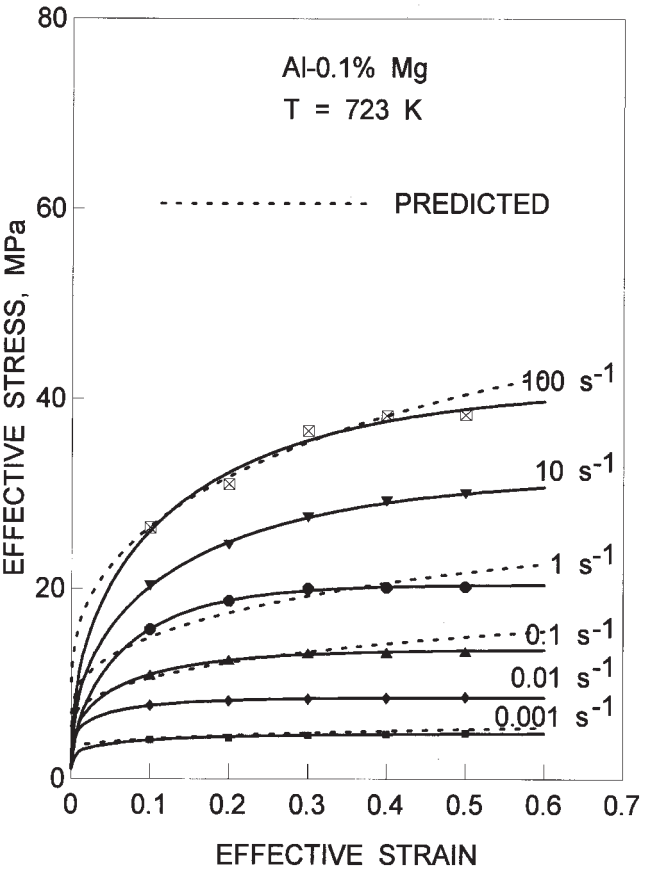

Fig. 7—Change in the current flow stress with strain at 723 K and different strain rates. The solid lines represent the optimization of the experimental data and the dotted lines the predictions of the constitutive equation proposed.

independent of $\dot{\varepsilon}$, it is observed that $\Phi_2 = 346$ MPa^2, whereas in the opposite case, $\Phi_2 = 312$ MPa^2. Thus, a decrease in the value of Φ_2 indicates an improvement in the prediction of the model.

Figure 9 illustrates the change in the component $\hat{\sigma}_D$ of the mechanical threshold with effective strain, as described by means of the generalized form of the Sah *et al.* law,[11] for different deformation conditions. The "structure" of the material represented by this parameter depends strongly on the strain applied, deformation temperature, and rate of straining. Thus, changes in the last two parameters may lead to equivalent "structure" conditions as shown from the curves obtained at 573 K–0.001 s^{-1} (curve b) and 823 K–100 s^{-1} (curve k). The latter curve, which is slightly displaced above the former, indicates the existence of a somewhat "harder" structure in which the increase in deformation temperature from 573 to 823 K has been compensated for also by increasing the strain rate from 0.001 to 100 s^{-1}.

Therefore, the use of the MTS as an internal state variable for the description of the constitutive behavior of this material has the advantage that arbitrary strain rate and temperature path changes can be readily dealt with. If a change in any of these variables occurs during deformation, the MTS is first recomputed, taking into consideration that changes in temperature will affect it through the parameters $\hat{\sigma}_{Ds}$, s_S, and s_D (Eqs. [17] and [18]), whereas changes in strain rate will induce changes in $\hat{\sigma}_{Ds}$, $\hat{\sigma}_D(\varepsilon_r)$, s_S ($\dot{\varepsilon}$, T), and s_D ($\dot{\varepsilon}$, T) also through Eqs. [17] and [18]. Finally, the current flow stress is computed from Eq. [6], taking into consideration the changes in temperature and strain rate.

An interesting result of the present investigation is that concerning the value of the normalized activation energy for the extrapolation of the saturation mechanical threshold to any combination of temperature and strain rate, g_{0Ds}, which, as reported in Table II, was found to be approximately equal to 0.5. Accordingly, it would be expected that in the temperature range of 573 to 823 K, ΔG_{0Ds} varied in the range of 150.1 to 124.8 kJ mol^{-1}. This range of values is close to 148 kJ mol^{-1}, a magnitude reported for self-diffusion and creep in pure aluminum, and 156 kJ mol^{-1}, the mean value usually reported as the activation for hot deformation of aluminum and its alloys.[15] This fact supports the indication that in the temperature range explored in the present work, the deformation of the material after achieving saturation would be controlled by both thermally activated climb processes of edge dislocations and motion of jogged screw dislocations.

Although the mechanical behavior of Al-Mg alloys have been widely reviewed by different authors,[16,17,18] only in a few instances have such investigations[7] been conducted from the standpoint of the MTS employing continuous stress-strain curves determined at constant temperature and strain rate.

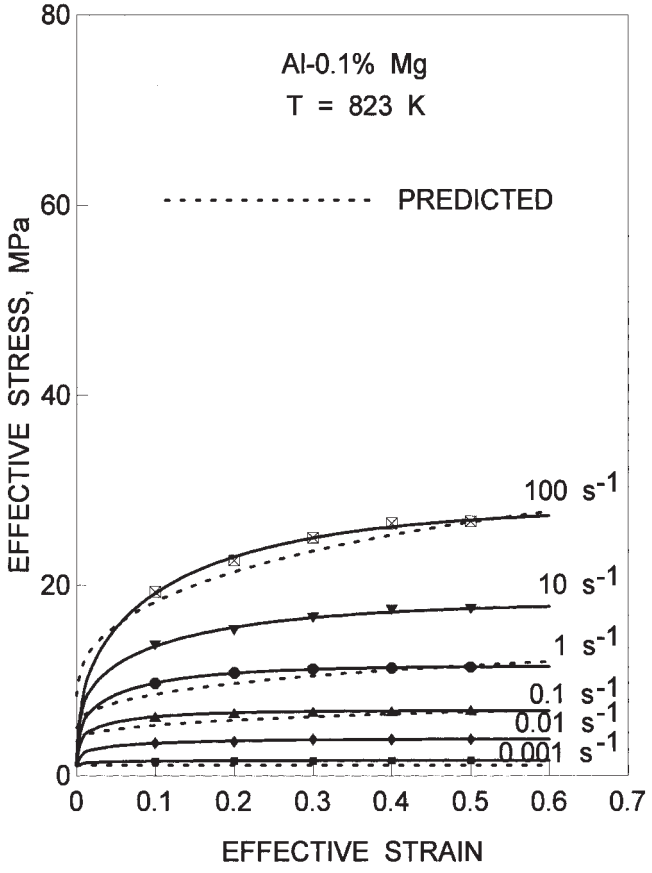

Fig. 8—Change in the current flow stress with strain at 823 K and different strain rates. The solid lines represent the optimization of the experimental data and the dotted lines the predictions of the constitutive equation proposed.

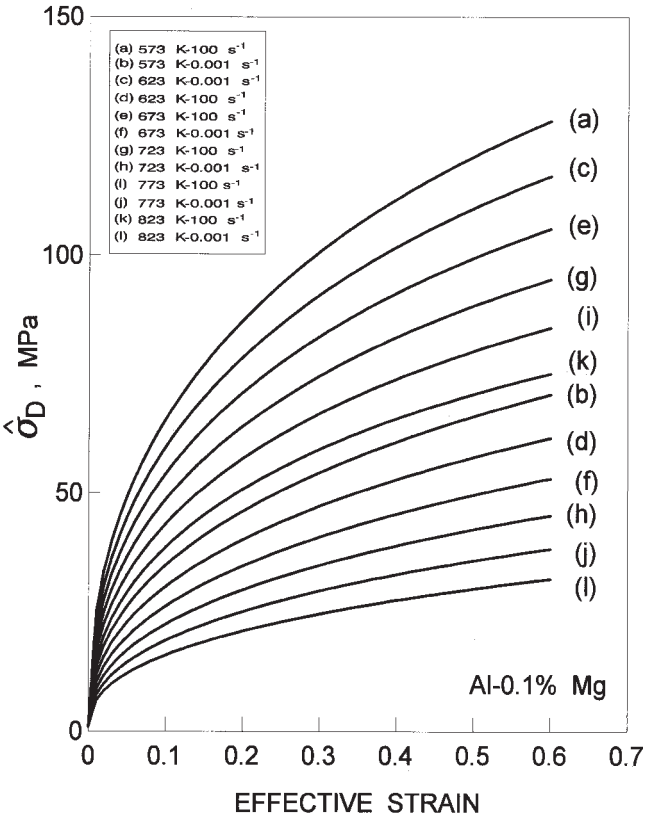

Fig. 9—Change in the component $\hat{\sigma}_D$ of the MTS with strain at different temperatures and strain rates.

Table II. Material Constants Involved in the Constitutive Description of the Material under Investigation

σ_a, MPa	0.75
$\dot{\varepsilon}_{KS}$, s^{-1}	2.96×10^4
g_{0S}	0.49
$\hat{\sigma}_s$, MPa	30.8
$\dot{\varepsilon}_{KD}$, s^{-1}	5.19×10^5
g_{0D}	0.55
ε_{r0}	1.05
ε_{r1}	1.19×10^{-2}
m_r	−0.63
$\hat{\sigma}_{KDs}$	0.014
$\dot{\varepsilon}_{KDs}$, s^{-1}	3.63×10^8
g_{0Ds}	0.5
n	0.43
k/$\mathbf{b}^3$	0.59

Particularly, for dilute Al-Mg alloys, it would be expected that during deformation at elevated temperatures, well polygonized subgrains were formed as the deformation applied increased and the saturation stress were achieved, as a consequence of the operation of dynamic recovery as the main restoration mechanism.

McQueen[17] has pointed out that rising the Mg content in these alloys causes parabolic hardening with the concentration exponent declining from 0.5 to 0.25 as the density of impurities increases. Also, this author reported that the activation energies for deformation were observed to increase steadily from approximately 143 to 160 $kJmol^{-1}$ as the Mg content increased from 0 to 5 wt pct. Such values are in agreement with previous findings[16,19] concerning the computation of this parameter, which reported values of 130 to 150 kJ mol^{-1} for Mg contents from 0 to 2 wt pct, which are in the range of the activation energies for the diffusion either of Al or Mg atoms. These values are also in very good agreement with the present results, regarding the value of the activation energy for deformation under steady-state conditions.

Also, as the Mg content increases, it would be expected that the substructure evolved from a refined cell arrangement to a different microstructure capable of accommodating the strain applied, reflected in a much higher dislocation density. As pointed out by Hughes and Liu,[20] as the Mg content increases beyond 4 wt pct, the microstructure can be described in terms of random dislocations and microbands, which, in turn, can be interpreted in terms of the organization of dislocations in a type of multi-Burgers vector Taylor lattice and the formation of dislocation domain boundaries between differently oriented regions of such lattices as precursors to the microbands. All these complex microstructural changes are bound to have a profound effect on the different constants that intervene in the constitutive description of the material, and therefore, more work is required in order to conduct similar analyses in other Al-Mg systems with higher Mg contents, to allow a consistent comparison of the results computed following a similar approach.

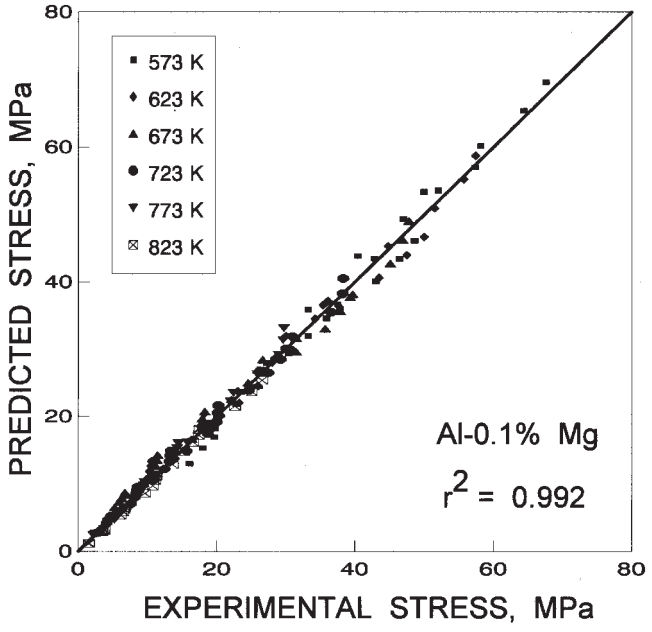

Fig. 10—Comparison between the experimental and calculated values of the flow stress; r^2 represents the coefficient of determination.

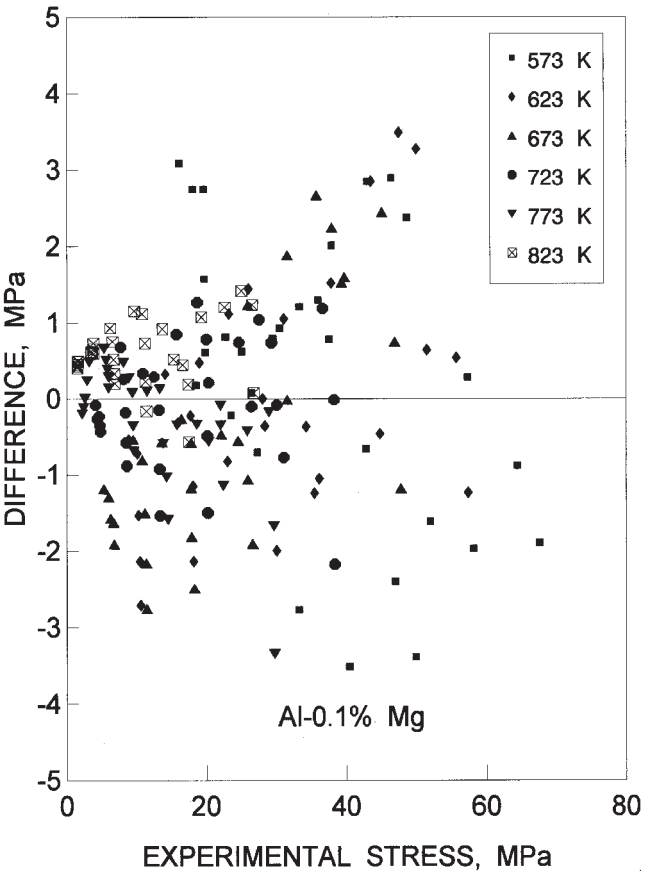

Fig. 11—Difference between the experimental and calculated values of the flow stress, as a function of the former.

Finally, it is important to point out that the constitutive description proposed here for the material investigated is able to reproduce the flow stress values quite accurately, as shown in Figures 10 and 11, which show the comparison between the experimental and predicted values of the flow stress and the difference between these two magnitudes as a function of the experimental flow stress, respectively. Particularly, in the latter figure, it can be appreciated that the maximum difference between the experimental and predicted flow stress values is less than ±4 MPa, which is observed for several data points at temperatures of 573 and 623 K, whereas the vast majority of the data points are in the region of ±3 MPa.

IV. CONCLUSIONS

The flow stress and work-hardening behavior of an aluminum-0.1 pct magnesium alloy deformed under hot-working conditions can be described satisfactorily on the basis of the MTS model, assuming that this parameter arises from the contribution of two different components: a first one, from the interaction between dislocations and solute atoms, $\hat{\sigma}_S$, and a second one from the interaction between the mobile and forest dislocations, $\hat{\sigma}_D$. Also, it has been determined that the evolution of this second component of the MTS can be satisfactorily described by means of the generalized form of the exponential-saturation law earlier proposed by Sah *et al*., assuming that the relaxation strain can be represented as a function of the strain rate, by means of a simple parametric relationship, which is consistent with a similar dependence of the athermal work-hardening rate on $\dot{\varepsilon}$ reported previously in the literature. The inclusion of the strain rate dependence of ε_r into the expression of the component $\hat{\sigma}_D$ of the MTS leads to an improvement in the accuracy of the prediction of the constitutive equation proposed, and therefore, it can be employed as a satisfactory approach for modeling the present data. It has been found that the experimental stress-strain data can be reproduced by the model with a maximum difference ±4 MPa.

ACKNOWLEDGMENTS

The present investigation has been carried out with the financial support of the Venezuelan National Fund for Science, Technology and Innovation (FONACIT), through Project No. S1-2000000642, and the financial support of the Scientific and Humanistic Development Council (CDCH), Universidad Central de Venezuela, through Project Nos. PI 08-17-2779-2000 and PG 08-17-4595-2000.

REFERENCES

1. H. Li, S. Saigal, P.T. Wang, and H.R. Piehler: *Int. J. Plasticity*, 1995, vol. 11 (4), pp. 331-45.
2. P.S. Follansbee and U.F. Kocks: *Acta Metall*., 1988, vol. 36, pp. 81-93.
3. H. Mecking and U.F. Kocks: *Acta Metall*., 1981, vol. 29, pp. 1865-75.
4. P.S. Follansbee and G.T Gray: *Metall. Trans. A*, 1989, vol. 20A, pp. 863-74.
5. S.R. Chen and G.T Gray III: *Metall. Mater. Trans. A*, 1996, vol. 27A, pp. 2994-3006.

6. G.T. Gray III, S.R. Chen, and K.S. Vecchio: *Metall. Mater. Trans. A*, 1999, vol. 30A, pp. 1235-47.
7. E.S. Puchi-Cabrera, C. Villalobos-Gutiérrez, and G. Castro-Fariñas: *J. Eng. Mater. Technol*., 2001, vol. 123, pp. 155-61.
8. E. Voce: *J. Inst. Met*., 1948, vol. 74, pp. 537-62
9. E. Voce: *Metallurgia*, 1955, vol. 51, pp. 219-26
10. U.F. Kocks: *J. Eng. Mater. Technol*., 1976, vol. 98, pp. 76-85.
11. J.P. Sah, G. Richardson, and C.M. Sellars: *J. Aust. Inst. Met*., 1969, vol. 14, p. 292.
12. U.F. Kocks, A.S Argon, and M.F. Ashby: *Progress in Materials Science*, Pergamon Press, Oxford, United Kingdom, 1975, vol. 19, p. 135.
13. *Hot Working Guide: A Compendium of Processing Maps*, Y.V.R.K. Prasad and S. Sasidhara, eds., ASM INTERNATIONAL, The Materials Information Society, Materials Park, OH, 1997.
14. P.M. Sutton: *Phys. Rev*., 1953, vol. 91, pp. 816-21.
15. J.J. Jonas, C.M. Sellars, and W.J. McG. Tegart: *Int. Metall. Rev*., 1969, vol. 14 (130), pp. 1-24.
16. H.J. McQueen and K. Conrod: in *Microstructural Control in Aluminum Alloys*, E.H. Chia and H.J. McQueen, eds., *TMS-AIME*, Warrandale, PA, 1986, pp. 197-219.
17. H.J. McQueen: in *Hot Deformation of Aluminum Alloys*, T.G. Langdon, H.D. Merchant, J.G. Morris, and M.A. Zaidi, eds., TMS, Warrandale, PA, 1991, pp. 31-54.
18. H.J. McQueen and J. Belling: *Can. Met. Q*., 2000, vol. 39 (4), pp. 483-92.
19. H.J. McQueen and N. Ryum: *Scand. J. Met*., 1985, vol. 14, pp. 183-94.
20. D.A. Hughes and Y.L. Liu: in *Hot Deformation of Aluminum Alloys*, T.G. Langdon, H.D. Merchant, J.G. Morris, and M.A. Zaidi, eds., TMS, Warrandale, PA, 1991, pp. 21-30.